© 2020. Published by The Company of Biologists Ltd | Development (2020) 147, dev189985. doi:10.1242/dev.189985

RESEARCH ARTICLE

Unveiling a novel function of CD9 in surface compartmentalization of oocytes

Naokazu Inoue*, Takako Saito and Ikuo Wada

ABSTRACT

Gamete fusion is an indispensable process for bearing offspring. In mammals, sperm IZUMO1–oocyte JUNO recognition essentially carries out the primary step of this process. In oocytes, CD9 is also known to play a crucial role in gamete fusion. In particular, microvilli biogenesis through CD9 involvement appears to be a key event for successful gamete fusion, because CD9-disrupted oocytes produce short and sparse microvillous structures, resulting in almost no fusion ability with spermatozoa. In order to determine how CD9 and JUNO cooperate in gamete fusion, we analyzed the molecular profiles of each molecule in CD9- and JUNO-disrupted oocytes. Consequently, we found that CD9 is crucial for the exclusion of GPI-anchored proteins, such as JUNO and CD55, from the cortical actin cap region, suggesting strict molecular organization of the unique surface of this region. Through distinct surface compartmentalization due to CD9 governing, GPI-anchored proteins are confined to the appropriate fusion site of the oocyte.

KEY WORDS: Oocyte, Fertilization, GPI-anchored proteins (GPI-APs), Microvilli, CD9, JUNO

INTRODUCTION

In multiple phases of mammalian gamete fusion, IZUMO1 (Inoue et al., 2005) and its receptor JUNO (also known as IZUMO1R) (Bianchi et al., 2014) are the well-documented first pair of gamete recognition factors of the spermatozoon and the ovum, respectively. We, as well as another group, have recently clarified the tertiary structures of the human IZUMO1-JUNO complex at atomic resolution (Aydin et al., 2016; Ohto et al., 2016). We have also shown that the initial gamete recognition step can be reconstituted in cultured cells expressing the *Izumo1* gene with oocytes (Inoue et al., 2013). As the cultured cells solely expressing the *Izumo1* gene lacked membrane fusion activity, IZUMO1-JUNO interaction is considered to be a recognition step before membrane fusion (Inoue et al., 2015); however, the detailed molecular mechanisms underlining gamete fusion remain elusive.

The oocyte surface (oolemma) in mammals is mainly divided into two areas: the microvilli-devoid region located on the surface of the cortical actin cap region, which anchors meiosis metaphase II chromosomes (Uraji et al., 2018), and the microvilli-rich region, in which the spermatozoon binds to the oocyte (Yanagimachi, 1994). Cluster of differentiation 9 (CD9), a member of the tetraspanin family of proteins, is required for accomplishing gamete fusion, as female CD9 mutants have been found to exhibit severely reduced litter size and gamete fusion ability (Kaji et al., 2000; Le Naour et al., 2000; Miyado et al., 2000). In 2007, Runge et al. first reported that CD9-disrupted oocytes have microvilli of altered size, thickness and density (Runge et al., 2007), and another group confirmed that CD9 deletion increased microvilli thickness (Benammar et al., 2017). Although there are discrepancies in the reports of the effects of CD9 deletion on microvilli density (Benammar et al., 2017; Miyado et al., 2008; Runge et al., 2007), oocyte CD9 is at least regarded as an indispensable factor for the formation of normal microvilli.

CD9 is known to interact with various proteins, such as integrins, and forms a dynamic complex termed the ‘tetraspanin web’ (Boucheix and Rubinstein, 2001). In particular, oocyte CD9 is strongly associated with CD315 (EWI-F; PTGFRN) and IGSF8 (EWI-2) (Runge et al., 2007); however, IGSF8 is not functional in the fertilization (Inoue et al., 2012). IGSF8 and CD315 bind directly to ezrin, radixin and moesin (ERM) through their cytoplasmic tails, finally linking to the actin filaments of the microvillous core (Sala-Valdés et al., 2006). Intriguingly, the CD9 homologues CD81 and CD82 regulate microvillus morphogenesis positively and negatively, respectively, by altering cortical actin cytoskeletal organization (Bari et al., 2011).

Another important aspect of CD9 is its association with fertilization. Utilizing adhesion force measurements, Jegou et al. reported that strong adhesion activity of the oocyte to the spermatozoon through the tetraspanin web to trigger sperm-egg fusion is impaired in CD9-null oocytes, whereas total frequency of gamete adhesion is increased (Jegou et al., 2011). In addition, Miyado et al. demonstrated that exosome-like CD9-containing vesicle release from an oocyte leads to spermatozoon fusion-facilitating activity (Miyado et al., 2008), although this observation may be controversial because their experiments have been found to be unreproducible by two independent research groups (Barraud-Lange et al., 2012; Gupta et al., 2009).

In the present study, we provide evidence indicating that a newly discovered CD9 physiological function enables exofacial exclusion of glycosylphosphatidylinositol (GPI)-anchored proteins (GPI-APs) from the cortical actin cap region in mouse oocytes.

RESULTS

Two oolemma factors, CD9 and JUNO, have independent behaviour in gamete fusion

We first examined the localization of CD9 and JUNO in mouse eggs using α-CD9 (MZ3) or α-JUNO (TH6) monoclonal antibodies 15 min after insemination (Fig. 1). As IZUMO1 relocates from the acrosomal cap to the whole head of the spermatozoa after acrosome reaction, acrosome-reacted (AR) spermatozoa were detected by α-IZUMO1 staining of the whole sperm head (Inoue et al., 2005; Inoue and Wada, 2018; Satouh et al., 2012). Both JUNO and CD9 on the egg were found to be concentrated in regions at which

Department of Cell Science, Institute of Biomedical Sciences, School of Medicine, Fukushima Medical University, 1 Hikarigaoka, Fukushima City, Fukushima 960-1295, Japan.

*Author for correspondence (n-inoue@fmu.ac.jp)

N.I., 0000-0002-6187-8293; T.S., 0000-0002-3969-9192; I.W., 0000-0001-5668-6994

Handling Editor: Haruhiko Koseki
Received 26 February 2020; Accepted 6 July 2020

Development (2020) 147, dev189985. doi:10.1242/dev.189985

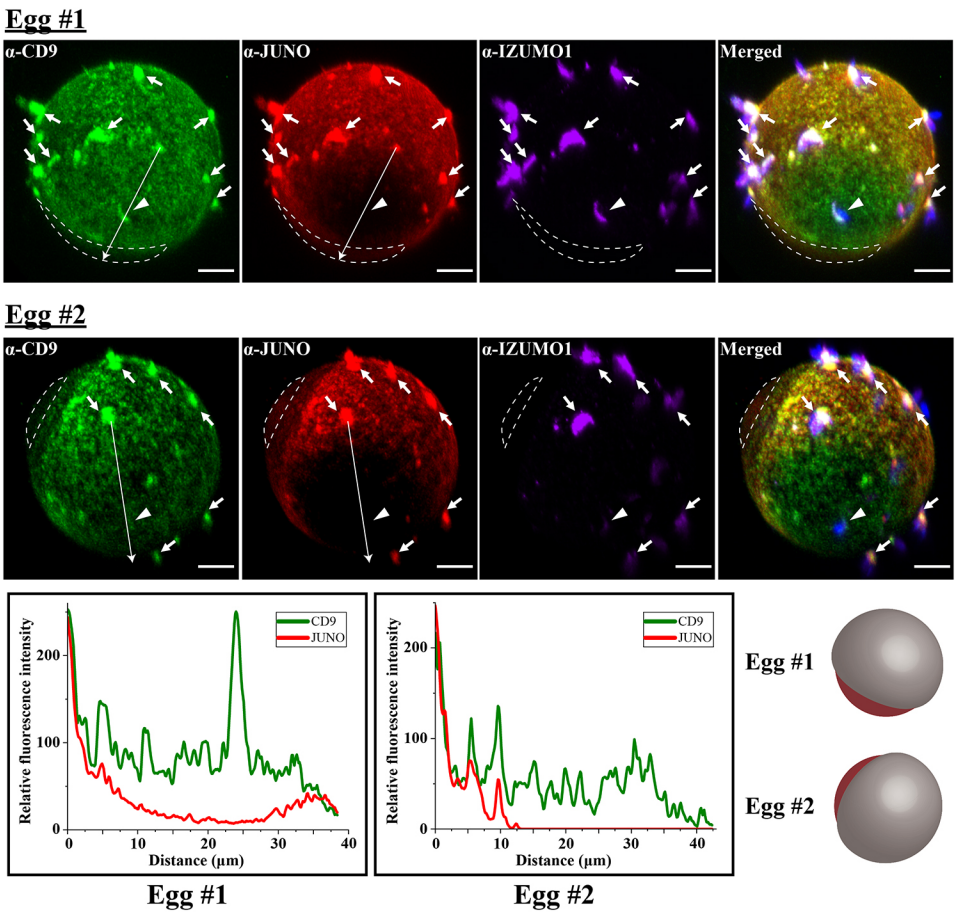

Fig. 1. Localization of oocyte CD9 and JUNO at the moment of sperm-egg fusion. Eggs were stained with MZ3-FITC (CD9: green), TH6-Alexa647 (JUNO: red), Mab125-Alexa546 (IZUMO1: purple) and Hoechst 33342 (nucleus: blue). Eggs were fixed 15 min after insemination. The arrows and arrowheads indicate spermatozoa bound to the oolemma and fused spermatozoon, respectively. The cortical actin cap is surrounded by a broken line. The schematic represents the position of the cortical actin cap region in red in each egg (bottom right panel). The relative fluorescence intensity in the long arrows of the CD9 and JUNO staining images in both eggs was analyzed using Fiji (graphs bottom left). Scale bars: 10 μm.

spermatozoa labelled with α-IZUMO1 antibody were bound (Fig. 1, arrows), which is consistent with previous reports (Inoue et al., 2015; Kaji et al., 2002; Ravaux et al., 2018). The crescent-shape staining pattern of IZUMO1 in Egg #1 shows a state occurring within 5 min of gamete fusion (Fig. 1, arrowheads) (Satouh et al., 2012). Interestingly, in the area where the sperm-egg fusion occurred, CD9 was still fully present, whereas JUNO had partially disappeared from the surface of the oocyte in concentric circles (Fig. 1, arrowheads). Regarding JUNO, this is a response observed immediately after fusion with a spermatozoon, implying that the polyspermy block system had been launched (Bianchi et al., 2014). In Egg #2, fertilization appeared to be at a later stage because the nucleus of the fused spermatozoon started swelling and IZUMO1 was almost absent (Fig. 1, middle panels, arrowheads). Profiles of the fluorescence intensity of CD9 and JUNO indicated that, although CD9 was still present in both eggs, Egg #2 entirely lost JUNO from around the gamete fusion site, whereas JUNO was still present in the Egg #1 surface, albeit at very low levels (Fig. 1, long arrows, left bottom panels). These results suggest that the molecular dynamics of CD9 and JUNO are differentially regulated, immediately following sperm-egg fusion.

Generation and analysis of CD9- and JUNO-disrupted mice

In order to analyze how CD9 and JUNO cooperate in fertilization, we generated CD9 and JUNO knockout mice using the CRISPR/Cas9 system. We designed a single guide RNA (sgRNA) to target the upstream domain of the second large extracellular loop for CD9, known as the functional domain (Zhu et al., 2002), or the initial methionine codon for the *Juno* gene (Fig. 2A). We then injected pX330-sgRNA plasmids into the pronuclei of fertilized eggs (Mashiko et al., 2013). Consequently, we obtained mouse lines in which 10 and 31 bases were deleted in CD9 and JUNO genomic DNA, respectively (Fig. 2A, red rectangles). Loss of CD9 or JUNO proteins in each knockout mouse line was confirmed by western blot analysis with α-CD9 (EM-04) or α-JUNO (12A5) monoclonal antibodies, respectively (Fig. 2B, Fig. S4). When expression levels of CD9 or JUNO proteins were examined from 20 eggs obtained from three independent mice, there was no significant difference in protein expression. JUNO showed smeared bands in the SDS-PAGE, implying that JUNO oocytes acquired post-translational modification (Fig. 2B).

We next performed an *in vitro* fertilization (IVF) assay to confirm the failure of gamete fusion, as previously reported (Bianchi et al., 2014; Kaji et al., 2000; Le Naour et al., 2000; Miyado et al., 2000). Both $Cd9^{-/-}$ and $Juno^{-/-}$ oocytes showed almost no fertilized eggs, whereas the fertilization rate of the wild-type oocytes was nearly 100% (Fig. 2C).

Next, we performed immunostaining analysis in living $Cd9^{-/-}$ and $Juno^{-/-}$ oocytes with specific monoclonal antibodies (Fig. 2D). CD9 or JUNO proteins were not observed on the surface of the $Cd9^{-/-}$ or $Juno^{-/-}$ oocytes, respectively (Fig. 2D, middle and bottom panels), although both proteins were detected on the surface of the wild-type oocytes (Fig. 2D, upper panels). Importantly, we noticed that in the $Cd9^{-/-}$ oocytes, JUNO localization was abnormal, i.e. although JUNO was seen in the cortical actin cap region lacking microvilli, as well as the microvilli-rich region, it was nearly absent from the cortical actin cap region in the wild-type oocytes (Fig. 2D, arrows).

Binding of recombinant IZUMO1 to $Cd9^{-/-}$ or $Juno^{-/-}$ oocytes

We previously showed that sperm-egg recognition/adhesion can be reconstituted in cultured cells expressing the *Izumo1* gene with

Development (2020) 147, dev189985. doi:10.1242/dev.189985

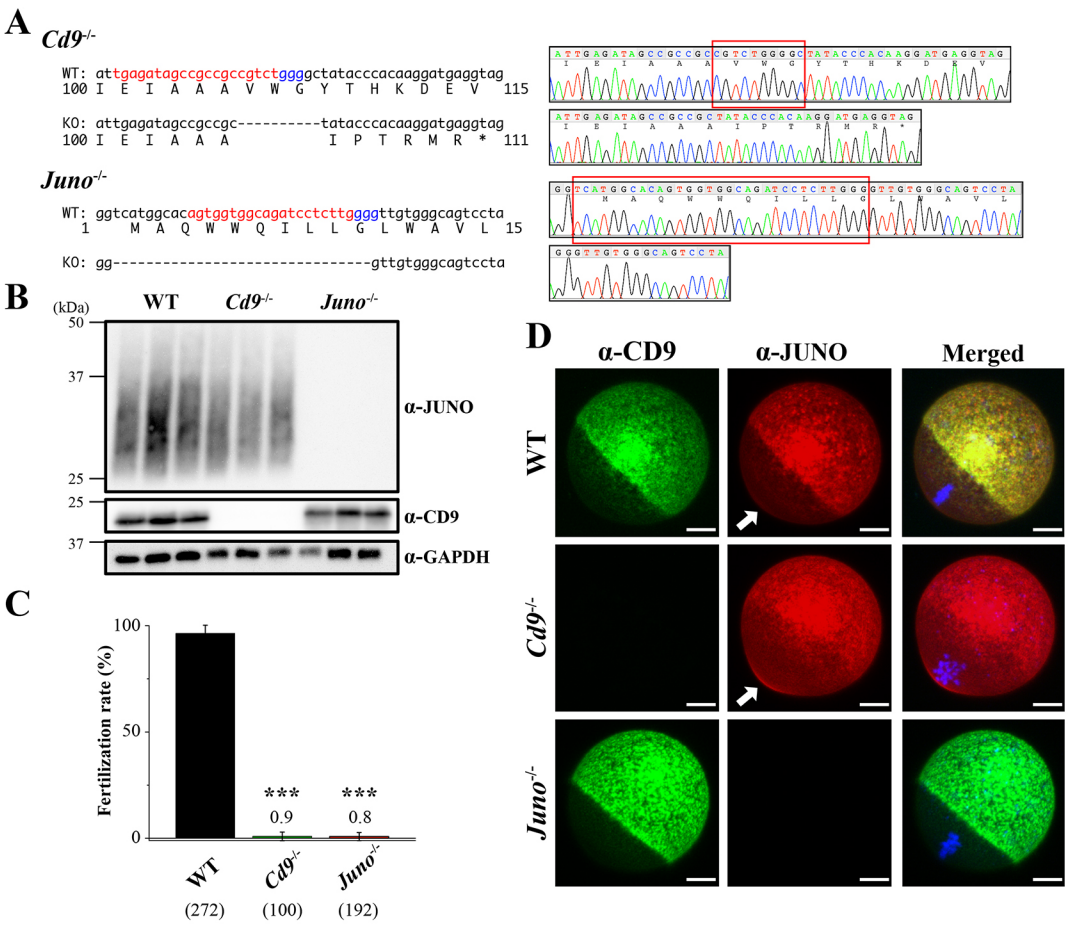

Fig. 2. Generation of *Cd9*$^{-/-}$ and *Juno*$^{-/-}$ mice. (A) Genome-editing using the CRISPR/Cas9 system. The red and blue letters show the target and protospacer adjacent motif (PAM) sequence, respectively (left panels). A DNA sequence chromatogram shows that the *Cd9*$^{-/-}$ and *Juno*$^{-/-}$ mice had a 10-base and 31-base deletion, respectively. The deleted sequences are boxed in red (right panels). (B) Western blot analysis of 20 oocyte lysates with 12A5 (JUNO) and EM-04 (CD9). Each lane represents a different individual wild-type (WT), *Cd9*$^{-/-}$ and *Juno*$^{-/-}$ mouse. Glyceraldehyde-3-phosphate dehydrogenase (GAPDH) was used as a loading control. (C) *In vitro* fertilization assay using WT, *Cd9*$^{-/-}$ and *Juno*$^{-/-}$ female oocytes (n=13, 5 and 12, respectively). The numbers in parentheses indicate the numbers of oocytes used. The error bars represent s.d. ***P<0.001 (paired two-tailed Student's t-test, compared with WT). (D) Immunostaining analysis of WT, *Cd9*$^{-/-}$ and *Juno*$^{-/-}$ oocytes with MZ3-FITC (CD9: green), TH6-Alexa647 (JUNO: red) and Hoechst 33342 (nucleus: blue). The arrows indicate the cortical actin cap region. Scale bars: 10 µm.

oocytes (Inoue et al., 2013). To evaluate the IZUMO1 binding ability of oocytes lacking CD9 or JUNO, we first measured the interaction of each oocyte to IZUMO1-PA- or IZUMO1-mCherry-expressing COS-7 (African green monkey kidney fibroblast-like cell line) cells. As shown in Fig. 3A, the *Cd9*$^{-/-}$ oocytes showed clear binding to IZUMO1-PA expressed in COS-7 cells, whereas bound cells were almost absent in Juno$^{-/-}$ oocytes, although the number of associated cells was reduced compared with those in the wild-type oocytes. The characteristic clustering of dimeric IZUMO1-mCherry at the contact site was observed as reported in a previous study (Fig. 3B, asterisks; Inoue et al., 2015). In *Cd9*$^{-/-}$ oocytes, however, the strong adhesion activity between the spermatozoon and oocyte is impaired (Jegou et al., 2011), although IZUMO1 recruitment kinetics is accelerated at the contact site (Chalbi et al., 2014). Thus, the lack of CD9 likely affects the tight binding phase of the IZUMO1 molecule resulting in the reduction of the number of binding cells. Next, to further characterize the IZUMO1 and JUNO interaction, recombinant IZUMO1-FC fusion protein (IZUMO1-FC) was produced in 293T cells. Fig. 3C shows that 5 µg ml^{-1} IZUMO1-FC bound to both wild-type and *Cd9*$^{-/-}$ oocytes; however, no binding was observed with *Juno*$^{-/-}$ oocytes because of the lack of IZUMO1-JUNO interaction. During this experiment, recombinant IZUMO1 staining was observed as densely clustered patches on the surface of the oocytes (Fig. 3C), which appeared to represent the bundled microvillous regions or more complex structures. Interestingly, IZUMO1-FC failed to bind to the cortical actin cap region, despite the obvious JUNO localization in the *Cd9*$^{-/-}$ oocytes (Fig. 3C). Taken together, the IZUMO1-JUNO interaction is not hindered by CD9 disruption; therefore, IZUMO1-JUNO and CD9 may be independent pathways for triggering sperm-egg fusion.

Surface structure of *Cd9*$^{-/-}$ and *Juno*$^{-/-}$ oocytes

We next considered the possibility that the aberrant JUNO distribution in the *Cd9*$^{-/-}$ oocytes may be caused by an impaired cortical actin cap structure. We observed the oocyte surface ultrastructure using scanning electron microscopy (SEM). As shown in Fig. 4A, there was no obvious distortion in the images of surface structure surrounding the cortical actin cap region in the *Cd9*$^{-/-}$ oocytes. All microvilli of *Cd9*$^{-/-}$ oocytes were shorter and less densely packed than those of the wild-type oocytes, as reported previously (Benammar et al., 2017; Runge et al., 2007). The SEM image of *Juno*$^{-/-}$ oocytes was not distinguishable from that of the wild-type oocytes. Consistently, phalloidin staining showed that F-actin was fully formed in this region, and there were no signs of

Development (2020) 147, dev189985. doi:10.1242/dev.189985

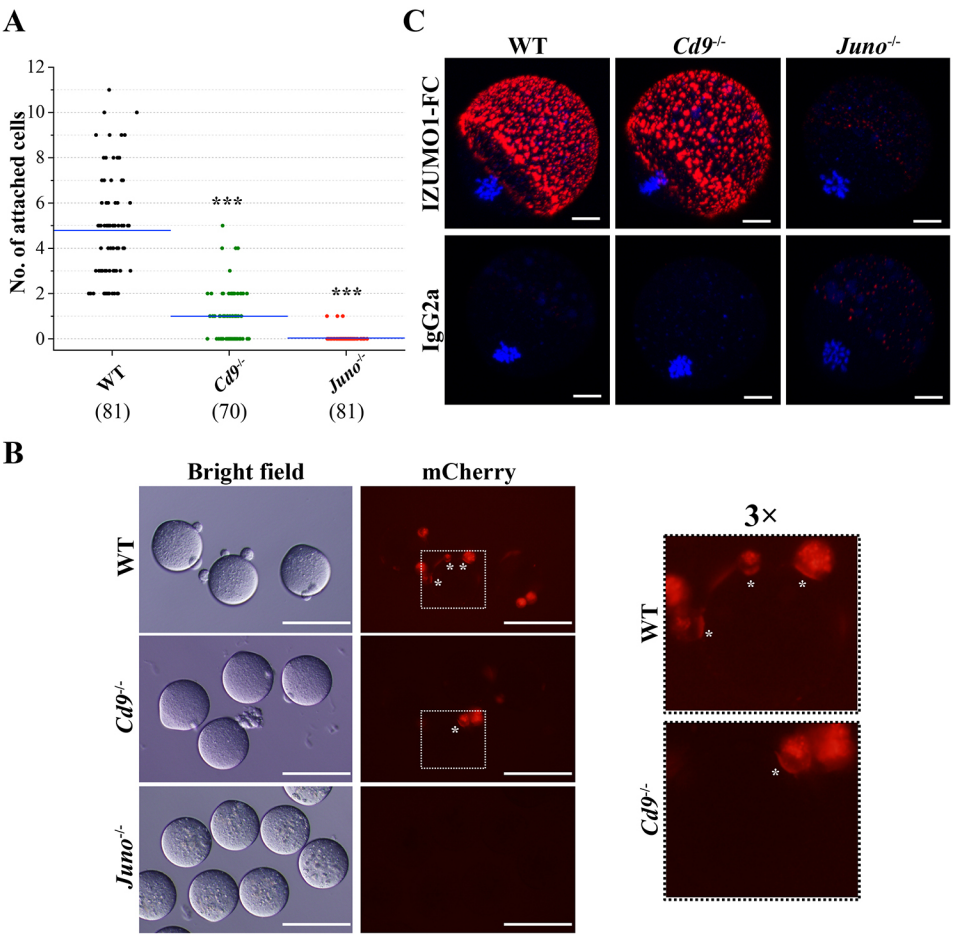

Fig. 3. *Cd9*$^{-/-}$ oocytes bind to recombinant IZUMO1, but not *Juno*$^{-/-}$ oocytes. (A) Cell-oocyte assay using an *Izumo1-PA* stable cell line. *Izumo1-PA*-expressing COS-7 cells were incubated with WT, *Cd9*$^{-/-}$ and *Juno*$^{-/-}$ oocytes. The numbers of attached COS-7 cells per oocyte from three independent experiments are shown. The numbers in parentheses indicate the numbers of oocytes examined, and the blue lines indicate the mean. ***P<0.001 (paired two-tailed Student's t-test, compared with WT). (B) Representative image of the cell-oocyte assay using an *Izumo1-mCherry* stably expressing cell line. A 3× magnified image of the white dashed boxed area is also shown on the right. The adhesion surface of COS-7 cells to the oocyte is indicated by asterisks. Scale bars: 100 µm. (C) Immunostaining of IZUMO1-FC recombinant protein. Zona-free WT, *Cd9*$^{-/-}$ and *Juno*$^{-/-}$ oocytes were incubated in TYH medium for 1 h with IZUMO1–FC and Hoechst 33342. Subsequently, they were incubated with Alexa Fluor 546-conjugated α-mouse IgG (red) to visualize them. Mouse IgG2a was used as an isotype control because FC fusion protein is derived from mouse IgG2a. Scale bars: 10 µm.

abnormality in the *Cd9*$^{-/-}$ oocytes (Fig. 4B). Indeed, the cortical actin cap was not disturbed by latrunculin B treatment, which inhibits the polymerization of monomeric actin, although patched distribution of CD9, integrin α6 and JUNO proteins was observed (Fig. S1). Thus, the cause of the aberrant JUNO distribution in the *Cd9*$^{-/-}$ oocytes is unlikely to be the cortical actin cap structure itself.

Impaired surface segregation of GPI-anchored proteins in *Cd9*$^{-/-}$ oocytes

Previous studies have shown that integrin α6 is most likely to be the *cis*-partner of CD9 through the tetraspanin web in oocytes (Boucheix and Rubinstein, 2001; Miyado et al., 2000). We therefore surmised that loss of CD9 might cause disturbance in integrin α6 localization. However, immunofluorescence experiments of the *Cd9*$^{-/-}$ oocytes indicated that integrin α6, as well as integrin β1, CD315 and CD81, were excluded from the cortical actin cap region (Fig. 5A and Fig. S2A-D). On the other hand, CD55, a GPI-AP (Alfieri et al., 2003), was incompletely excluded from the cortical actin cap region in *Cd9*$^{-/-}$ oocytes, with the pattern being very much similar to that of JUNO (Fig. S2E). When the fraction of oocytes with proper segregation of JUNO and integrin α6 was quantified, we found that all *Cd9*$^{-/-}$ oocytes showed incomplete surface compartmentalization of JUNO, which invaded the cortical actin cap region from the rest of the area. This was in contrast to the integrin α6 compartmentalization that was almost the same as that in the wild-type oocytes (Fig. 5A, graph). These observations suggest that GPI-APs, which tend to be incorporated in lipid rafts on the plasma membrane, can invade the cortical actin cap region.

It is known that tetraspanins (CD9, etc.) are localized to the cholesterol-depletion-resistant membrane microdomain (non-lipid raft), whereas GPI-APs (JUNO, etc.) are present in the cholesterol-rich microdomain (lipid raft) (Buschiazzo et al., 2013). These two types of proteins appear to be difficult to come across in association with each other owing to their properties. However, this mode of interaction between two proteins in non-lipid raft and lipid raft domains has been reported previously, and it was abrogated by treatment with methyl-β-cyclodextrin (MβCD), a cholesterol-depleting reagent (Wang et al., 2007). As the treatment lowers lateral diffusion of CD9, as revealed by single molecule analysis, the frequency of molecular interaction could be reduced (Espenel et al., 2008). Thus, to determine whether the membrane raft integrity is required for regulation of CD9-mediated GPI-APs dynamics, we analyzed molecular localization under the cholesterol depletion. First, we determined optimized concentration of MβCD for live imaging of oocytes, and chose 2 mM MβCD (Fig. S3A). As seen in Fig. S3B, MβCD treatment showed normal molecular compartmentalization of JUNO in the wild-type oocytes, and did not improve exclusion of JUNO in the cortical actin cap region of the *Cd9*$^{-/-}$ oocytes, although clustered punctate structures of CD9, integrin α6 and JUNO proteins appeared as observed for latrunculin B treatment (Fig. S1).

To further characterize this property, we performed fluorescence recovery after photobleaching (FRAP) experiments using α-JUNO antibodies labelled with a fluorophore to monitor diffusion of endogenous JUNO proteins. As expected, the recovery was almost negligible in the wild-type oocytes after photobleaching the cortical actin cap region. However, in the corresponding region of the *Cd9*$^{-/-}$

Development (2020) 147, dev189985. doi:10.1242/dev.189985

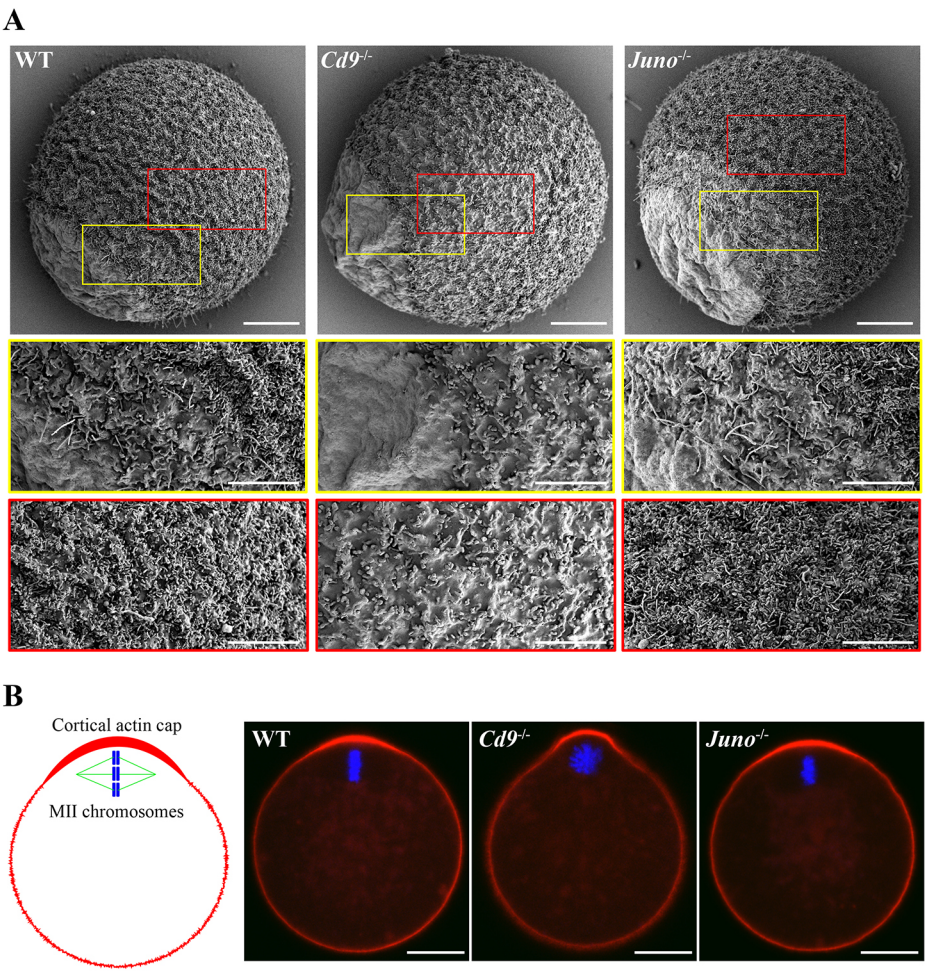

Fig. 4. SEM image and phalloidin staining of WT, *Cd9*$^{-/-}$ and *Juno*$^{-/-}$ oocytes. (A) SEM images of WT, *Cd9*$^{-/-}$ and *Juno*$^{-/-}$ oocytes. Red and yellow boxes correspond to each magnified image. Scale bars: 10 µm (top); 5 µm (bottom). (B) WT, *Cd9*$^{-/-}$ and *Juno*$^{-/-}$ oocytes were stained with BODIPY 558/568 phalloidin (F-actin: red) and Hoechst 33342 (nucleus: blue) after fixation. Scale bars: 20 µm.

oocytes, the recovery was significantly observed, albeit at a slower rate compared with experiments using the surface of cultured cells (Fig. 5B and Movie 1). We obtained similar results with CD55 (Movie 2). Thus, this suggests that CD9 is required to establish the proper cortical actin cap with strict filtration function that excludes GPI-APs.

Finally, we analyzed sperm-oocyte binding in the cortical actin cap region of the *Cd9*$^{-/-}$ oocytes. In this assay, we employed IZUMO1-mCherry and acrosomal enhanced green fluorescent protein (Acr-EGFP) double transgenic spermatozoa to distinguish between acrosome intact (AI) (Fig. 5C, double positive, yellow) and AR (Fig. 5C, IZUMO1-mCherry single positive, red) spermatozoa. The distribution of bound spermatozoa was evaluated by integrin α6 localization because, even in *Cd9*$^{-/-}$ oocytes, integrin α6 shows normal compartmentalization (Fig. 5A and Fig. S2A). Astonishingly, as seen in the images in Fig. 5C, 10 min after insemination with zona-free oocytes, the majority of the bound spermatozoa did not undergo acrosome reaction, suggesting that the plasma membrane binding factors of spermatozoa bind to oolemma before sperm-egg fusion, despite a non-physiological event. The number of spermatozoa bound to *Cd9*$^{-/-}$ oolemma significantly decreased not only in the AI but also, more importantly in the AR spermatozoa (Fig. 5C, arrows). There was no statistical difference between number of spermatozoa bound to the cortical actin cap region in the wild-type and *Cd9*$^{-/-}$ oocytes; however, multiple bound AI spermatozoa were rarely seen in *Cd9*$^{-/-}$ oocytes (Fig. 5C, image of *Cd9*$^{-/-}$ oocyte, arrowheads). AR spermatozoa bound to the cortical actin cap were exceptionally rare [wild-type: 0.23% (7/2997 bound spermatozoa), *Cd9*$^{-/-}$: 0.22% (3/1366 bound spermatozoa)], suggesting that JUNO, which is localized in the cortical actin cap region in *Cd9*$^{-/-}$ oocytes, is somehow maintained in an inactive state for binding of IZUMO1 (Fig. 3C). Thus, we presume that the cortical actin cap region is functionally organized by multiple systems other than CD9 regulations, to which CD9 compartmentalization-unaffected transmembrane type plasma membrane binding factors (e.g. integrin) may be committed before IZUMO1-JUNO interaction, to exclude spermatozoa from there.

DISCUSSION

The results of the current study show that the characteristic cortical actin cap surface of oocytes is insufficiently formed in *Cd9*$^{-/-}$ oocytes. We therefore propose that CD9 is required for regulating the molecular compartmentalization of GPI-APs on the cortical actin cap surface. Given that spermatozoa are unable to bind to the cortical actin cap surface which is adjacent to chromosomes, this unique zone on the cortical actin cap has to be completely organized through CD9 involvement before gamete recognition (Fig. 6).

The cortical actin cap region of oocytes is a less characterized structure. In the current study, although the surface images of the cortical actin cap of CD9-deficient oocytes were indistinguishable from wild-type oocytes when observed by SEM, further FRAP experiments clearly indicated that CD9-deficient oocytes lacked the property to exclude GPI-APs, JUNO and CD55, from the cortical actin cap region (Fig. 5B, Movies 1 and 2). Because, unlike the

Development (2020) 147, dev189985. doi:10.1242/dev.189985

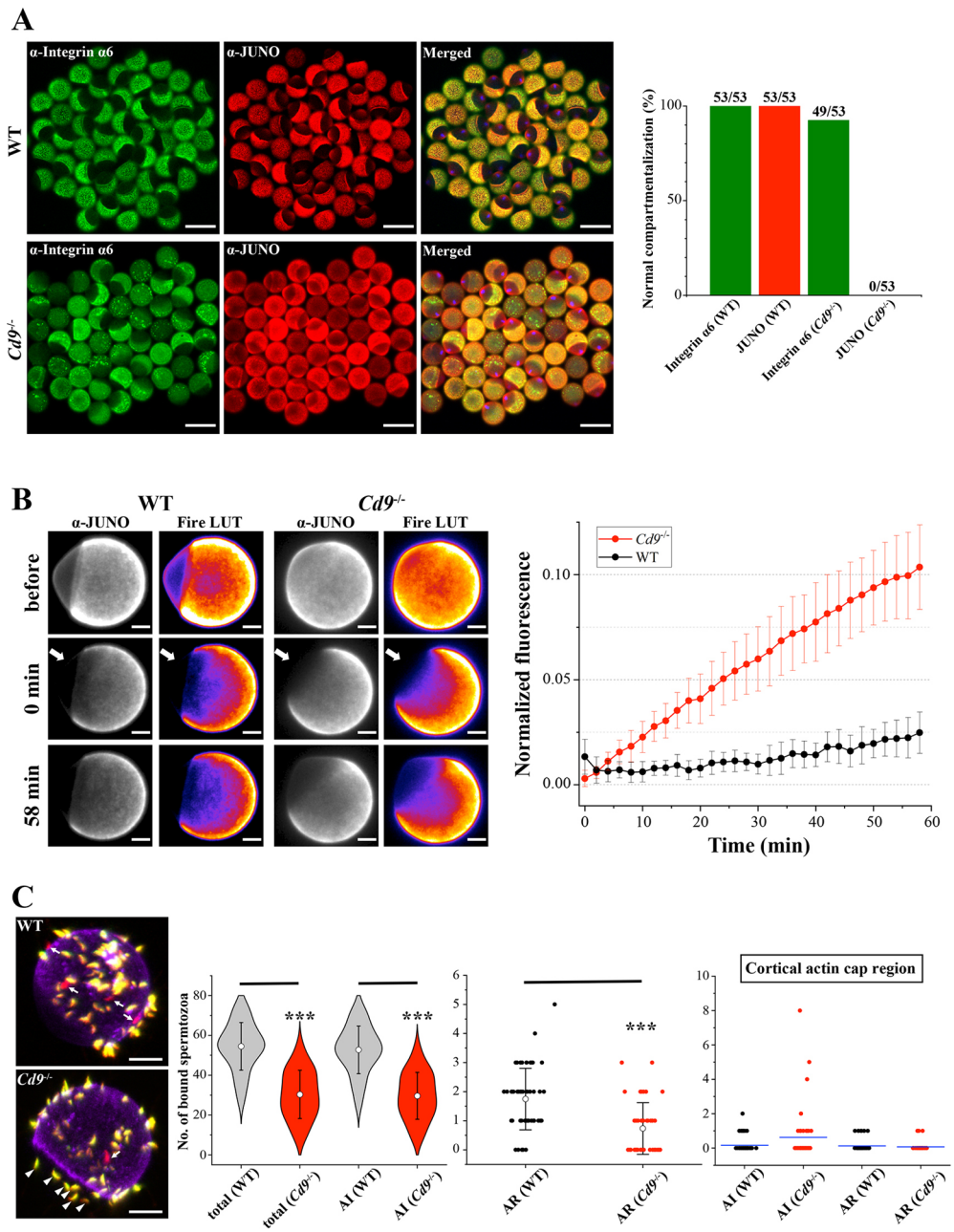

Fig. 5. Infiltration of JUNO in the cortical actin cap region of *Cd9*$^{-/-}$ oocytes. (A) Immunofluorescence evaluation of JUNO. WT and *Cd9*$^{-/-}$ oocytes were incubated with GoH3-Alexa546 (integrin α6: green), TH6-Alexa647 (JUNO: red) and Hoechst 33342 (nucleus: blue), and the number of cells showing exclusion of JUNO from the cortical actin cap (three individuals, 53 oocytes) is shown on the right. Images consisting of 100-120 *z*-stacks were taken at 1 µm intervals with a 20× objective lens, and then 3D images were reconstructed. Each image of a representative focal plane is shown. Scale bars: 100 µm. We define the normal compartmentalization of integrin α6 or JUNO as the oocytes in which the fluorescence signal was confined in the microvilli-rich area but not in the cortical actin cap region, and visually assigned each oocyte. The graph indicates fractions of oocytes with the normal compartmentalization of each molecule. (B) FRAP experiments. The zona-free WT or *Cd9*$^{-/-}$ oocytes stained with TH6-Alexa647 (JUNO) were photobleached in the cortical actin cap region (arrows). The recovery was recorded as described in the Materials and Methods section at 2 min intervals over 58 min. Images of a whole oocyte before and after photobleaching are shown (left panels). Oocytes are shown in grayscale and Fire LUT of Fiji. Scale bars: 10 µm. The graph shows the value of normalized fluorescence of cortical actin cap region in WT and *Cd9*$^{-/-}$ oocytes. Error bars show the 95% confidence interval (*n*=8 each). (C) Sperm-oocyte binding assay. Acr-EGFP spermatozoa lose their green fluorescence after acrosome reaction, whereas IZUMO1–mCherry remains. Therefore, AI and AR spermatozoa were visualized in EGFP and mCherry double positive (green and red: yellow), and mCherry single positive (red, arrows), respectively. The distribution of the number of bound spermatozoa to the oolemma for total (AI and AR) and the AI spermatozoa is represented as a violin plot. That of the AR spermatozoa and the cortical actin cap region bound spermatozoa is represented as a dot plot (four individuals; WT: 55 eggs; *Cd9*$^{-/-}$: 45 eggs). White circle shows the mean. Error bars indicate s.d. ***P<0.001 (paired two-tailed Student's *t*-test, compared with WT). In terms of the cortical actin cap-bound spermatozoa, the staining pattern of GoH3-Alexa647 (integrin α6: purple) was used to specify the cortical actin cap, and the spermatozoa bound to the cortical actin cap (arrowheads in image) were counted (right graph). The blue lines indicate the mean. Scale bars: 20 µm.

GPI-APs that are only tethered to the outer plasmalemmal leaflet, the membrane spanning proteins, such as integrin α6 and β1, CD315 and CD81, were still excluded from the cortical actin cap region of *Cd9*$^{-/-}$ oocytes (Fig. S2), the unknown outer leaflet domains other than the lipid raft have to participate actively in the surface compartmentalization through the commitment of CD9.

Development (2020) 147, dev189985. doi:10.1242/dev.189985

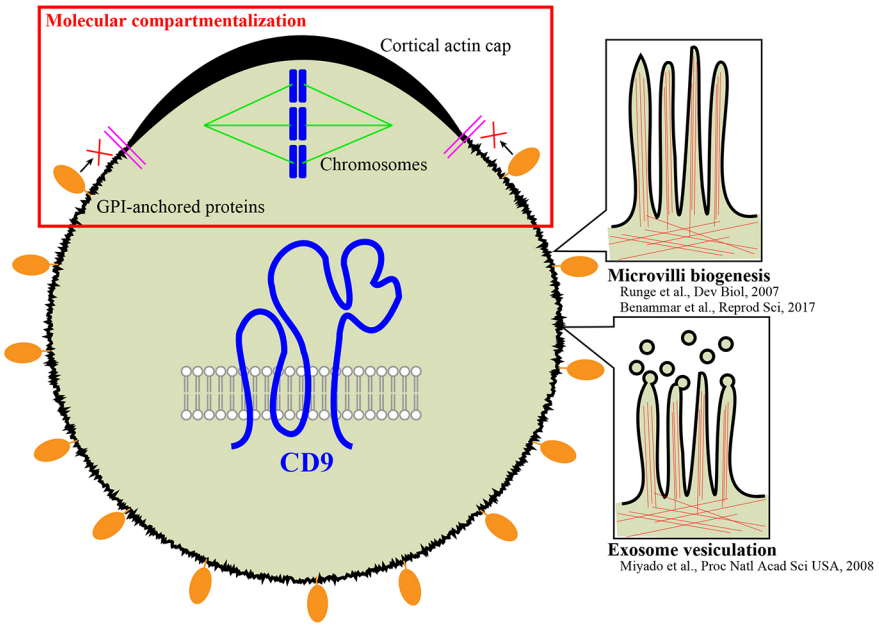

Fig. 6. Proposed diagram for CD9 functions in oocyte. Oocyte physiological functions in fertilization through CD9 involvement have been previously reported, including 'microvilli biogenesis' and 'exosome vesiculation'. In the present study, we propose that CD9 plays a crucial role in the 'molecular compartmentalization' of GPI-APs, which excludes GPI-APs from the cortical actin cap region. Once this segregation system is disturbed, GPI-APs such as JUNO can exist in the cortical actin cap region so that spermatozoa may bind there. In this case, the fertilization process may not be properly coordinated and, importantly, the secure partition of genome DNA may be disturbed because this region is physically very close to the chromosomes. Thus, in order to avoid any possibility of incorrect merging of the gametes, this system must be functional, even though IZUMO1 protein is unable to bind to the cortical actin cap surface of CD9-deficient oocytes presenting JUNO. Pink double bars represent compartmental boundaries.

Nucleation of actin in the cortex is known to be generated by Arp2/3 (Actr2/3) formed by the Ran^{GTP} gradient via the Cdc42-N-WASP or Rac-WAVE pathway (Yi et al., 2013). There are no reports that CD9 is involved in either pathway. In turn, incomplete exclusion of GPI-APs indicates that the exofacial surface in the cortical actin cap region is not as tightly packed as that in the wild-type; thus, diffusion of molecules on the outer plasmalemmal leaflet is less strictly limited. Our model also implies that the surface of the cortical actin cap region can be tightly coated with unknown molecule(s) or use macromolecular crowding to exclude inappropriate molecules such as JUNO from the region (Kuznetsova et al., 2014). Identification of the novel molecules that cooperate with CD9 to exclude GPI-APs in the cortical actin cap region should help determine the importance of CD9 in fertilization.

CD81, a homologue of CD9, has a large intramembrane cavity for the uptake of cholesterol within its transmembrane region, and is kept in a closed (cholesterol-bound) conformation until formation of a complex with CD19, *cis*-partner of CD81 (Zimmerman et al., 2016). It is well known that the GPI-APs have a preference for gathering in a lipid raft, which consists of microdomains enriched in cholesterol and sphingolipids. Interestingly, cholesterol depletion using MβCD in mouse oocytes has been reported to show a decrease in fertilization rate (Buschiazzo et al., 2013). However, cholesterol is less likely to maintain appropriate surface compartmentalization of GPI-APs through the involvement of CD9, because the compartmentalization of GPI-APs in the cortical actin cap was not influenced by MβCD treatment (Fig. S3). Furthermore, a recently-published study provided supporting evidence that CD9 spontaneously undergoes transitions between the open and closed conformations without cholesterol involvement, unlike CD81 (Umeda et al., 2020).

It is noteworthy that JUNO, which had exuded into the cortical actin cap in CD9-deficient oocytes, was incapable of binding to the recombinant IZUMO1 (Figs 2D and 3C). There are two possibilities for this: (1) IZUMO1-JUNO binding in oocytes requires another molecule existing in the microvilli, such as a secondary IZUMO1 receptor as we had previously claimed (Inoue et al., 2015); or (2) IZUMO1 is unable to interact with JUNO because of the steric hindrance or embedding with other molecule(s) in the cortical actin cap region. The former possibility may be less likely because the IZUMO1-JUNO complex was co-crystallized (Aydin et al., 2016; Ohto et al., 2016). We therefore think that the latter possibility is more plausible. As chromosomes are confined underneath the cortical actin cap, the establishment of a dense coat on the outer leaflet may help physically protect the elaborate post-fertilization processes.

Therefore, this study shows that, in order to accomplish fertilization properly, tetraspanin CD9 contributes to multiple physiological functions including microvilli biogenesis, exosome vesiculation and a novel 'molecular compartmentalization' in mammalian oocytes (Fig. 6). It remains elusive how multiple molecular mechanisms coordinate to operate appropriate fertilization; however, we believe it indicates that, in general, CD9 plays an important role in cluster-induced curvature generation in microvilli or exosome biogenesis (Umeda et al., 2020). A new insight into molecular signalling and interaction thorough tetraspanin involvement would greatly advance understanding of the elaborate molecular mechanisms of gamete recognition and fusion.

MATERIALS AND METHODS

Mice

B6D2F1 and ICR mice (*Mus musculus*) were purchased from Japan SLC. The B6D2F1 mouse strain was used as wild type in all experiments. IZUMO1 knockout (Inoue et al., 2005), IZUMO1-mCherry transgenic (Satouh et al., 2012) and Acr-EGFP (Nakanishi et al., 1999) mice were kindly provided by Osaka University. All animal studies were approved by the Animal Care and Use Committee of Fukushima Medical University, Japan, and performed under the guidelines and regulations of Fukushima Medical University.

Antibodies

An α-mouse IZUMO1 monoclonal antibody (Mab125) was conjugated to Alexa Fluor 647 (1:100). FITC-conjugated α-mouse CD9 monoclonal (MZ3, 1:1000, 124808), Alexa Fluor 647-labelled α-mouse JUNO monoclonal (TH6, 1:2000, 125110), Alexa Fluor 647-labelled α-mouse CD55 monoclonal (RIKO-3, 1:500, 131805) and unlabelled α-mouse JUNO (12A5, 1:500, 125002) monoclonal antibodies were purchased from BioLegend. Alexa Fluor 546- and 647-labelled α-mouse integrin α6 monoclonal (GoH3) antibodies were purchased from Santa Cruz Biotechnology (1:200, sc-19622AF546) and BioLegend (1:100, 313609),

Development (2020) 147, dev189985. doi:10.1242/dev.189985

respectively. FITC-labelled α-mouse integrin β1 monoclonal (HMb1-1, 1:100, AB_2572449) and unlabelled α-mouse CD9 (EM-04, 1:1000, AB_11155997) monoclonal antibodies were purchased from Thermo Fisher Scientific. Unlabelled α-mouse GAPDH (5A12, 1:500, 016-25523) and α-mouse CD81 (Eat2, 1:200, MCA1846AA) monoclonal antibodies were purchased from FUJIFILM Wako Pure Chemical Corporation and Bio-Rad, respectively. Unlabelled α-mouse CD315 polyclonal antibody (1:100, AF4495) was purchased from R&D Systems. Recombinant IZUMO1-FC (1:150), α-mouse CD81 monoclonal and α-mouse CD315 polyclonal antibodies were detected by secondary Alexa Fluor 546-labelled α-mouse IgG (Thermo Fisher Scientific, 1:250, A11030), Alexa Fluor 647-labelled α-Armenian hamster IgG (Jackson ImmunoResearch, 1:250, 127-035-160) and Alexa Fluor 647-labelled α-Sheep IgG (Jackson ImmunoResearch, 1:250, 713-605-147), respectively.

Fluorescence imaging for fixed eggs

Superovulation was induced in each female mouse (>8 weeks old) by injecting 7.5 IU of equine chorionic gonadotropin (eCG) and 7.5 IU of human chorionic gonadotropin (hCG) at 48 h intervals. Sixteen hours after hCG injection, oocytes were collected from the oviduct and placed in 50 µl of TYH medium. The zona pellucida was removed from the oocytes via treatment with 1.0 mg ml^{-1} of collagenase (FUJIFILM Wako Pure Chemical Corporation) (Yamatoya et al., 2011). Zona-free oocytes were incubated with 0.5 µg ml^{-1} MZ3-FITC and 0.25 µg ml^{-1} TH6-Alexa647 with 1 µg ml^{-1} of Hoechst 33342 (Thermo Fisher Scientific) for 1 h at 37°C in TYH medium. Mouse spermatozoa were collected from the cauda epididymis and capacitated *in vitro* for 1.5 h in a 200 µl drop of TYH medium with 0.5 µg ml^{-1} Mab125 that was covered with mineral oil. Then, 5×10^5 spermatozoa ml^{-1} was inseminated in the oocytes for 15 min at 37°C with 5% CO_2. After the eggs were washed several times in TYH medium by transferring spots of oocytes containing media, the eggs were fixed with 4% paraformaldehyde and 0.5% polyvinylpyrrolidone (PVP) in PBS for 30 min at room temperature, then observed in glass-bottom dishes (No. 0, MatTek Corporation). A 100× oil-immersion objective (numeric aperture 1.49) was used to capture confocal images with an A1R microscope (Nikon). The pinhole was set at 3.0 airy unit. For 3D reconstruction, 100-120 fluorescent images were taken at 1 µm intervals on the *z*-axis, and then 3D images were reconstructed using the built-in software NIS-Elements ver. 4.3 (Nikon).

Generation of $Cd9^{-/-}$ and $Juno^{-/-}$ mice

A pair of oligonucleotides (5′-CACCGTGAGATAGCCGCCGCCGTCT-3′ and 5′-AAACAGACGGCGGCGGCTATCTCAC-3′ for CD9; 5′-CACC-GAGTGGTGGCAGATCCTCTTG-3′ and 5′-AAACCAAGAGGATCTG-CCACCACTC-3′ for JUNO) as guide sequences were annealed and cloned into a *Bbs*I cut pX330 vector (Addgene plasmid #42230). pX330 plasmid DNA was purified and diluted into 5 mM Tris-HCl (pH 7.4)/0.1 mM EDTA of a final 5 ng $µl^{-1}$ concentration. Plasmid DNA was injected into the pronuclei of fertilized eggs with glass capillaries attached to a micromanipulator (FemtoJet, Eppendorf). After microinjection, the zygotes were transferred and cultured in KSOM (ARK Resource) at 37°C with 5% CO_2, and two-cell embryos were transferred into pseudopregnant ICR female mice. F3 and F4 generation mice were used for the experiments, and all genotyping was performed by PCR on tail-tip DNA using CD9 5′-TGTGGGTATAGCCCCAGACG-3′ for wild-type or 5′-CATCCTTG-TGGGTATAGCGG-3′ for KO and 5′-CCCTCATGATGCTGGTTGGT-3′ as forward and reverse primers, respectively, and JUNO 5′-CAAGAGG-ATCTGCCACCACT-3′ for wild-type or 5′-TAGGACTGCCCACAACC-CTG-3′ for KO and 5′-AGATCCATTCCTTGCCTGGC-3′ as forward and reverse primers, respectively. CD9 and JUNO knockout mice have been deposited at the RIKEN BioResource Research Centre [RIKEN BRC (https://web.brc.riken.jp/en/); accession numbers RBRC10274 and RBRC10276, respectively].

Western blot analysis

Superovulated oocytes were washed three times using PBS, treated with SDS-sample buffer [62.5 mM Tris-HCl (pH 6.8), 2% SDS, 10% glycerol] and a protease inhibitor cocktail (FUJIFILM Wako Pure Chemical Corporation), then used for western blotting under non-reduced conditions. The membranes were probed with primary antibodies [1 µg ml^{-1} α-CD9 (EM-04), 1 µg ml^{-1} α-JUNO (12A5) and 1 µg ml^{-1} α-GAPDH (5A12)] followed by secondary antibodies conjugated to HRP (Jackson ImmunoResearch, 1:5000, 115-036-062 and 112-006-143). Chemiluminescence reactions were performed with ECL Prime (Merck Millipore).

In vitro fertilization

B6D2F1 mouse spermatozoa were collected from the cauda epididymis and were capacitated *in vitro* for 1.5 h in a 200 µl drop of TYH medium that was covered with mineral oil. Superovulation was induced in each female mouse (>8 weeks old) as described above. Oocytes were collected from the oviduct, placed in 100 µl of TYH medium and incubated with 2×10^5 spermatozoa ml^{-1} at 37°C with 5% CO_2. After 4 h insemination, the oocytes were washed with TYH medium and the fertilization rate was evaluated by pronuclear formation.

Fluorescence imaging for live oocytes

Zona-free oocytes were prepared as described above. For the actin depolymerization treatment, zona-free oocytes were incubated with 10 µM latrunculin B (Merck) or 0.2% DMSO in TYH medium for 1 h at 37°C in 5% CO_2 in advance (Runge et al., 2007). The oocytes were then incubated with 0.5 µg ml^{-1} MZ3-FITC and 0.5 µg ml^{-1} TH6-Alexa647, or 5 µg ml^{-1} IZUMO1-FC or 1 µg ml^{-1} GoH3-Alexa546 and 0.5 µg ml^{-1} TH6-Alexa647 with 1 µg ml^{-1} of Hoechst 33342 for 1 h at 37°C in 5% CO_2 in TYH medium. After being washed several times in TYH medium, the oocytes were placed in FHM medium (Merck Millipore) and then observed on glass-bottom dishes (No. 0, MatTek). The observation conditions were the same as those described above in 'Fluorescence imaging for fixed eggs' and the samples were kept at 37°C.

Cell-oocyte assay

The IZUMO1-PA or -mCherry stably expressing COS-7 cells were treated with 5 mM EDTA-PBS at 37°C for 10 min, washed three times with PBS, centrifuged at 6000 ***g*** for 1 min and suspended in TYH medium (LSI Medience Corporation). Zona-free oocytes were incubated with the collected cells at 37°C in the TYH medium for 30 min. The oocytes were then washed and moved to drops of TYH medium, and the attached cells were counted under an inverted microscope (Olympus IX71). COS-7 cells were obtained from RIKEN BRC. This cell line has been authenticated as mycoplasma free by PCR.

Purification of IZUMO-FC fusion protein

The mature domain of mouse IZUMO1 (residues 22-319) cDNA without the secretion signal peptide region (residues 1-21) was expressed fusing with the CH2 and CH3 domains of the mouse IgG2a heavy chain and the hinge region from the expression vector pCMV6-AC-FC-S (OriGene). This construct uses a human interleukin 2 (IL2) leader sequence at the N terminus. For expression, 293T cells were transiently transfected with the IZUMO1-FC DNA using Polyethyleneimine 'Max' (Polysciences). These cells were maintained in 100 ml of DMEM supplemented with 2% fetal bovine serum, 1 mM sodium pyruvate, 1× non-essential amino acids (Nacali Tesque), 2 mM L-glutamine, 1000 units of penicillin and 1 mg of streptomycin at 37°C. The medium was collected after 4 days, and debris was filtrated using a 0.45 µm filter before loading on HiTrap rProtein A FF columns (GE Healthcare). The column was washed with 20 mM phosphate buffer (pH 7.0), eluted with 0.1 M sodium citrate (pH 3.0) and neutralized with 160 mM Tris-HCl (pH 9.0). Peak fractions were pooled and protein concentration measured using the Bradford protein assay. Finally, the protein purity was judged using SDS-PAGE.

SEM

Zona-free oocytes were prepared as described above, and placed on poly-L-lysine-coated cover glass for 30 s at room temperature. Primary fixation was performed in 4% paraformaldehyde, 2.5% glutaraldehyde, 2 mM $CaCl_2$ and 0.5% PVP in 250 mM HEPES buffer (pH 7.2). After fixation for 3 h at 4°C, the samples were washed with PBS three times and transferred into 2% osmium tetroxide in PBS at 4°C for 1 h. The samples were then dehydrated

in an ethanol series and dried in liquid CO_2 using a critical point drying apparatus (JCPD-5; JEOL). Next, the samples were transferred onto a stub with silver paste plus thinner and coated with osmium by an HPC-1SW coater (Shinku Device). An SU8220 SEM (Hitachi) was used for imaging according to the manufacturer's protocol.

Phalloidin staining of zona-free oocytes

Zona-free oocytes were fixed in 4% paraformaldehyde and 0.5% PVP in PBS for 30 min, then permeabilized with 0.25% Triton X-100 and 0.5% PVP in PBS for 20 min. After washing with FHM medium three times, the oocytes were incubated in FHM medium with 5 units ml^{-1} BODIPY 558/568 phalloidin (Thermo Fisher Scientific) and 1 µg ml^{-1} Hoechst 33342 for 10 min, followed by washing three times in FHM medium. The oocytes were then placed in FHM medium on glass-bottom dishes (No. 0) and imaged using a Nikon A1R confocal microscope equipped with 405- and 561-nm laser lines using a 100× oil-immersion objective lens.

MβCD treatment in zona-free oocytes

Zona-free oocytes were incubated with the appropriate antibodies and 1 µg ml^{-1} of Hoechst 33342 in TYH medium for 90 min, then treated with 2 mM MβCD (Sigma-Aldrich) in FHM medium for 30 min at 37°C to deplete cholesterol (Buschiazzo et al., 2013). After washing with FHM medium three times, the oocytes were placed in FHM medium on glass-bottom dishes (No. 0) and imaged using a Nikon A1R confocal microscope equipped with a 100× oil-immersion objective at 37°C.

FRAP

FRAP analysis of the oocytes was carried out as previously described (Nagaya et al., 2008). After immunostaining with 0.5 µg ml^{-1} TH6-Alexa647 (JUNO) (BioLegend, 1:1000, 125110) or 1 µg ml^{-1} RIKO-3-Alexa647 (CD55) (BioLegend, 1:500, 131805) for 2 h, the oocytes were washed three times in TYH medium and then placed in FHM medium on glass-bottom dishes (No. 0). The oocytes were kept at 37°C. A spot in the actin cap region was photobleached with a 640-nm laser from the Nikon A1R confocal microscope through a 60× water-immersion objective lens (numeric aperture 1.27) at 0.026 mW, and the recovery of the fluorescence was monitored at 2 min intervals. Fluorescence intensity before photobleaching was used to normalize the intensity during recovery.

Sperm-oocyte binding assay

Spermatozoa from IZUMO1-mCherry and Acr-EGFP double transgenic mice (*Izumo1* null genetic background) (Satouh et al., 2012) were collected from the cauda epididymis, and were capacitated *in vitro* for 2 h in a 200 µl drop of TYH medium that was covered with mineral oil. Zona-free oocytes were prepared as described above and incubated with 1 µg ml^{-1} α-mouse integrin α6 antibody (GoH3-Alexa647) (BioLegend, 1:100, 313609) for 90 min at 37°C in 5% CO_2 in TYH medium. After being washed with TYH medium three times, the oocytes were incubated with 5×10^5 spermatozoa ml^{-1} for 10 min at 37°C with 5% CO_2. The eggs were fixed with 4% paraformaldehyde and 0.5% PVP in PBS for 30 min at room temperature, then placed in FHM medium on glass-bottom dishes (No. 0) and imaged using a Nikon A1R confocal microscope equipped with a 60× water-immersion objective lens. The numbers of bound spermatozoa were counted.

Image and statistical analyses

All image and statistical analyses were performed using the open source software Fiji (Schindelin et al., 2012) and OriginPro 2020 (Light Stone), respectively.

Acknowledgements

We thank Drs Yuhkoh Satouh and Ken Sato (Gunma University) for thoughtful discussions.

Competing interests

The authors declare no competing or financial interests.

Author contributions

Conceptualization: N.I., I.W.; Methodology: N.I., T.S., I.W.; Validation: N.I.; Formal analysis: N.I.; Investigation: N.I., T.S.; Resources: N.I., T.S.; Data curation: N.I.; Writing - original draft: N.I.; Writing - review & editing: N.I., T.S., I.W.; Visualization: N.I.; Supervision: N.I., I.W.; Project administration: N.I.; Funding acquisition: N.I., T.S., I.W.

Funding

This work was supported by the Japan Society for the Promotion of Science (KAKENHI grants JP18H02453 to N.I., JP17K15128 to T.S. and JP17K07311 to I.W.), as well as by a research grant from the Takeda Science Foundation (to N.I.) and the joint research programme of the Institute for Molecular and Cellular Regulation, Gunma University (19014 to N.I.).

Supplementary information

Supplementary information available online at
https://dev.biologists.org/lookup/doi/10.1242/dev.189985.supplemental

References

Alfieri, J. A., Martin, A. D., Takeda, J., Kondoh, G., Myles, D. G. and Primakoff, P. (2003). Infertility in female mice with an oocyte-specific knockout of GPI-anchored proteins. *J. Cell Sci.* **116**, 2149-2155. doi:10.1242/jcs.00430

Aydin, H., Sultana, A., Li, S., Thavalingam, A. and Lee, J. E. (2016). Molecular architecture of the human sperm IZUMO1 and egg JUNO fertilization complex. *Nature* **534**, 562-565. doi:10.1038/nature18595

Bari, R., Guo, Q., Xia, B., Zhang, Y. H., Giesert, E. E., Levy, S., Zheng, J. J. and Zhang, X. A. (2011). Tetraspanins regulate the protrusive activities of cell membrane. *Biochem. Biophys. Res. Commun.* **415**, 619-626. doi:10.1016/j.bbrc.2011.10.121

Barraud-Lange, V., Chalas Boissonnas, C., Serres, C., Auer, J., Schmitt, A., Lefèvre, B., Wolf, J.-P. and Ziyyat, A. (2012). Membrane transfer from oocyte to sperm occurs in two CD9-independent ways that do not supply the fertilising ability of Cd9-deleted oocytes. *Reproduction* **144**, 53-66. doi:10.1530/REP-12-0040

Benammar, A., Ziyyat, A., Lefèvre, B. and Wolf, J.-P. (2017). Tetraspanins and mouse oocyte microvilli related to fertilizing ability. *Reprod. Sci.* **24**, 1062-1069. doi:10.1177/1933719116678688

Bianchi, E., Doe, B., Goulding, D. and Wright, G. J. (2014). Juno is the egg Izumo receptor and is essential for mammalian fertilization. *Nature* **508**, 483-487. doi:10.1038/nature13203

Boucheix, C. and Rubinstein, E. (2001). Tetraspanins. *Cell. Mol. Life Sci.* **58**, 1189-1205. doi:10.1007/PL00000933

Buschiazzo, J., Ialy-Radio, C., Auer, J., Wolf, J.-P., Serres, C., Lefèvre, B. and Ziyyat, A. (2013). Cholesterol depletion disorganizes oocyte membrane rafts altering mouse fertilization. *PLoS ONE* **8**, e62919. doi:10.1371/journal.pone.0062919

Chalbi, M., Barraud-Lange, V., Ravaux, B., Howan, K., Rodriguez, N., Soule, P., Ndzoudi, A., Boucheix, C., Rubinstein, E., Wolf, J. P. et al. (2014). Binding of sperm protein Izumo1 and its egg receptor Juno drives Cd9 accumulation in the intercellular contact area prior to fusion during mammalian fertilization. *Development* **141**, 3732-3739. doi:10.1242/dev.111534

Espenel, C., Margeat, E., Dosset, P., Arduise, C., Le Grimellec, C., Royer, C. A., Boucheix, C., Rubinstein, E. and Milhiet, P.-E. (2008). Single-molecule analysis of CD9 dynamics and partitioning reveals multiple modes of interaction in the tetraspanin web. *J. Cell Biol.* **182**, 765-776. doi:10.1083/jcb.200803010

Gupta, S., Primakoff, P. and Myles, D. G. (2009). Can the presence of wild-type oocytes during insemination rescue the fusion defect of CD9 null oocytes? *Mol. Reprod. Dev.* **76**, 602. doi:10.1002/mrd.21040

Inoue, N. and Wada, I. (2018). Monitoring dimeric status of IZUMO1 during the acrosome reaction in living spermatozoon. *Cell Cycle* **17**, 1279-1285. doi:10.1080/15384101.2018.1489181

Inoue, N., Ikawa, M., Isotani, A. and Okabe, M. (2005). The immunoglobulin superfamily protein Izumo is required for sperm to fuse with eggs. *Nature* **434**, 234-238. doi:10.1038/nature03362

Inoue, N., Nishikawa, T., Ikawa, M. and Okabe, M. (2012). Tetraspanin-interacting protein IGSF8 is dispensable for mouse fertility. *Fertil. Steril.* **98**, 465-470. doi:10.1016/j.fertnstert.2012.04.029

Inoue, N., Hamada, D., Kamikubo, H., Hirata, K., Kataoka, M., Yamamoto, M., Ikawa, M., Okabe, M. and Hagihara, Y. (2013). Molecular dissection of IZUMO1, a sperm protein essential for sperm-egg fusion. *Development* **140**, 3221-3229. doi:10.1242/dev.094854

Inoue, N., Hagihara, Y., Wright, D., Suzuki, T. and Wada, I. (2015). Oocyte-triggered dimerization of sperm IZUMO1 promotes sperm-egg fusion in mice. *Nat. Commun.* **6**, 8858. doi:10.1038/ncomms9858

Jegou, A., Ziyyat, A., Barraud-Lange, V., Perez, E., Wolf, J. P., Pincet, F. and Gourier, C. (2011). CD9 tetraspanin generates fusion competent sites on the egg membrane for mammalian fertilization. *Proc. Natl. Acad. Sci. USA* **108**, 10946-10951. doi:10.1073/pnas.1017400108

Kaji, K., Oda, S., Shikano, T., Ohnuki, T., Uematsu, Y., Sakagami, J., Tada, N., Miyazaki, S. and Kudo, A. (2000). The gamete fusion process is defective in eggs of Cd9-deficient mice. *Nat. Genet.* **24**, 279-282. doi:10.1038/73502

Kaji, K., Oda, S., Miyazaki, S. and Kudo, A. (2002). Infertility of CD9-deficient mouse eggs is reversed by mouse CD9, human CD9, or mouse CD81; polyadenylated mRNA injection developed for molecular analysis of sperm-egg fusion. *Dev. Biol.* **247**, 327-334. doi:10.1006/dbio.2002.0694

Kuznetsova, I. M., Turoverov, K. K. and Uversky, V. N. (2014). What macromolecular crowding can do to a protein. *Int. J. Mol. Sci.* **15**, 23090-23140. doi:10.3390/ijms151223090

Le Naour, F., Rubinstein, E., Jasmin, C., Prenant, M. and Boucheix, C. (2000). Severely reduced female fertility in CD9-deficient mice. *Science* **287**, 319-321. doi:10.1126/science.287.5451.319

Mashiko, D., Fujihara, Y., Satouh, Y., Miyata, H., Isotani, A. and Ikawa, M. (2013). Generation of mutant mice by pronuclear injection of circular plasmid expressing Cas9 and single guided RNA. *Sci. Rep.* **3**, 3355. doi:10.1038/srep03355

Miyado, K., Yamada, G., Yamada, S., Hasuwa, H., Nakamura, Y., Ryu, F., Suzuki, K., Kosai, K., Inoue, K., Ogura, A. et al. (2000). Requirement of CD9 on the egg plasma membrane for fertilization. *Science* **287**, 321-324. doi:10.1126/science.287.5451.321

Miyado, K., Yoshida, K., Yamagata, K., Sakakibara, K., Okabe, M., Wang, X., Miyamoto, K., Akutsu, H., Kondo, T., Takahashi, Y. et al. (2008). The fusing ability of sperm is bestowed by CD9-containing vesicles released from eggs in mice. *Proc. Natl. Acad. Sci. USA* **105**, 12921-12926. doi:10.1073/pnas.0710608105

Nagaya, H., Tamura, T., Higa-Nishiyama, A., Ohashi, K., Takeuchi, M., Hashimoto, H., Hatsuzawa, K., Kinjo, M., Okada, T. and Wada, I. (2008). Regulated motion of glycoproteins revealed by direct visualization of a single cargo in the endoplasmic reticulum. *J. Cell Biol.* **180**, 129-143. doi:10.1083/jcb.200704078

Nakanishi, T., Ikawa, M., Yamada, S., Parvinen, M., Baba, T., Nishimune, Y. and Okabe, M. (1999). Real-time observation of acrosomal dispersal from mouse sperm using GFP as a marker protein. *FEBS Lett.* **449**, 277-283. doi:10.1016/S0014-5793(99)00433-0

Ohto, U., Ishida, H., Krayukhina, E., Uchiyama, S., Inoue, N. and Shimizu, T. (2016). Structure of IZUMO1-JUNO reveals sperm-oocyte recognition during mammalian fertilization. *Nature* **534**, 566-569. doi:10.1038/nature18596

Ravaux, B., Favier, S., Perez, E. and Gourier, C. (2018). Egg CD9 protein tides correlated with sperm oscillations tune the gamete fusion ability in mammal. *J. Mol. Cell Biol.* **10**, 494-502. doi:10.1093/jmcb/mjy005

Runge, K. E., Evans, J. E., He, Z.-Y., Gupta, S., McDonald, K. L., Stahlberg, H., Primakoff, P. and Myles, D. G. (2007). Oocyte CD9 is enriched on the microvillar membrane and required for normal microvillar shape and distribution. *Dev. Biol.* **304**, 317-325. doi:10.1016/j.ydbio.2006.12.041

Sala-Valdés, M., Ursa, A., Charrin, S., Rubinstein, E., Hemler, M. E., Sánchez-Madrid, F. and Yáñez-Mó, M. (2006). EWI-2 and EWI-F link the tetraspanin web to the actin cytoskeleton through their direct association with ezrin-radixin-moesin proteins. *J. Biol. Chem.* **281**, 19665-19675. doi:10.1074/jbc.M602116200

Satouh, Y., Inoue, N., Ikawa, M. and Okabe, M. (2012). Visualization of the moment of mouse sperm-egg fusion and dynamic localization of IZUMO1. *J. Cell Sci.* **125**, 4985-4990. doi:10.1242/jcs.100867

Schindelin, J., Arganda-Carreras, I., Frise, E., Kaynig, V., Longair, M., Pietzsch, T., Preibisch, S., Rueden, C., Saalfeld, S., Schmid, B. et al. (2012). Fiji: an open-source platform for biological-image analysis. *Nat. Methods* **9**, 676-682. doi:10.1038/nmeth.2019

Umeda, R., Satouh, Y., Takemoto, M., Nakada-Nakura, Y., Liu, K., Yokoyama, T., Shirouzu, M., Iwata, S., Nomura, N., Sato, K. et al. (2020). Structural insights into tetraspanin CD9 function. *Nat. Commun.* **11**, 1606. doi:10.1038/s41467-020-15459-7

Uraji, J., Scheffler, K. and Schuh, M. (2018). Functions of actin in mouse oocytes at a glance. *J. Cell Sci.* **131**, jcs218099. doi:10.1242/jcs.218099

Wang, X.-Q., Yan, Q., Sun, P., Liu, J.-W., Go, L., McDaniel, S. M. and Paller, A. S. (2007). Suppression of epidermal growth factor receptor signaling by protein kinase C-alpha activation requires CD82, caveolin-1, and ganglioside. *Cancer Res.* **67**, 9986-9995. doi:10.1158/0008-5472.CAN-07-1300

Yamatoya, K., Ito, C., Araki, M., Furuse, R. and Toshimori, K. (2011). One-step collagenase method for zona pellucida removal in unfertilized eggs: easy and gentle method for large-scale preparation. *Reprod. Med. Biol.* **10**, 97-103. doi:10.1007/s12522-011-0075-8

Yanagimachi, R. (1994). *Mammalian Fertilization*. New York: Raven Press, Ltd.

Yi, K., Rubinstein, B. and Li, R. (2013). Symmetry breaking and polarity establishment during mouse oocyte maturation. *Philos. Trans. R. Soc. Lond. B Biol. Sci.* **368**, 20130002. doi:10.1098/rstb.2013.0002

Zhu, G. Z., Miller, B. J., Boucheix, C., Rubinstein, E., Liu, C. C., Hynes, R. O., Myles, D. G. and Primakoff, P. (2002). Residues SFQ (173-175) in the large extracellular loop of CD9 are required for gamete fusion. *Development* **129**, 1995-2002.

Zimmerman, B., Kelly, B., McMillan, B. J., Seegar, T. C. M., Dror, R. O., Kruse, A. C. and Blacklow, S. C. (2016). Crystal structure of a full-length human tetraspanin reveals a cholesterol-binding pocket. *Cell* **167**, 1041-1051.e1011. doi:10.1016/j.cell.2016.09.056

Supplementary Information

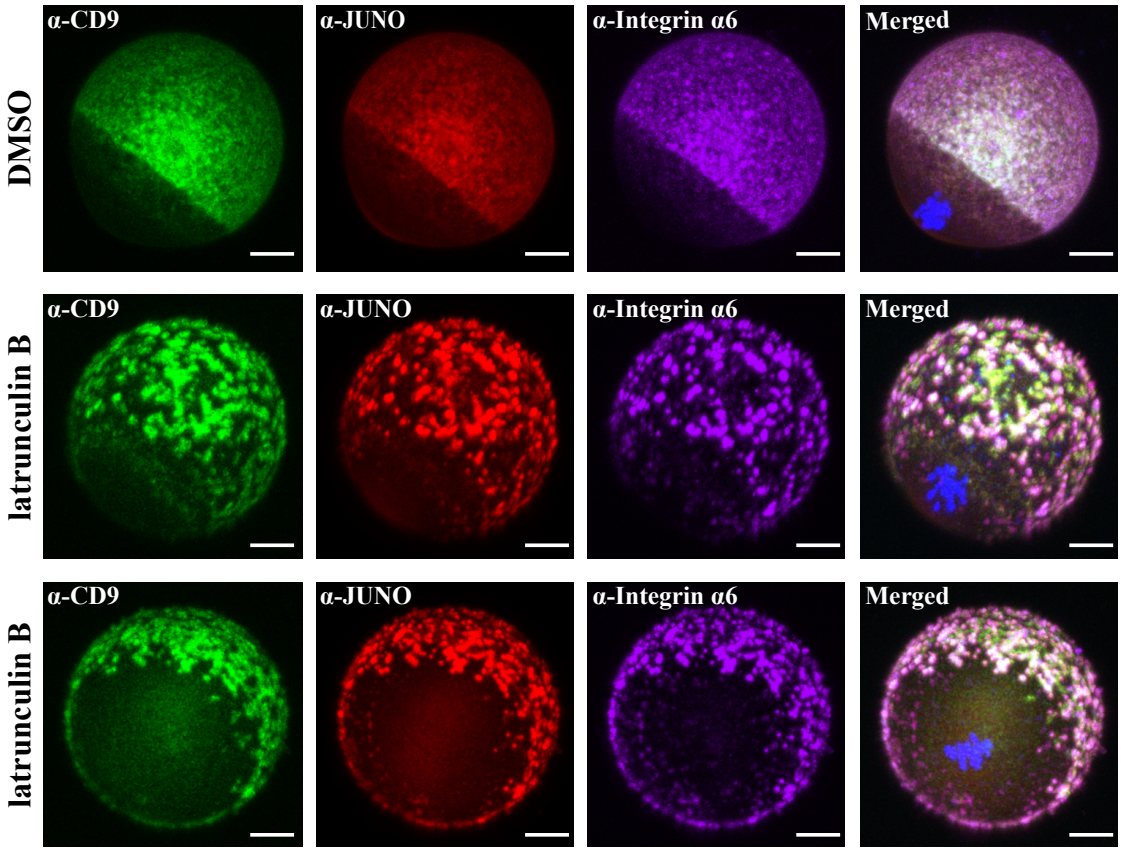

Fig. S1. Latrunculin B treatment in oocytes.

Immunostaining analysis of oocytes after being treated with latrunculin B. The oocytes were treated with 10 μM latrunculin B in TYH medium for 1 hour, then incubated with 0.5 μg ml^{-1} MZ3-FITC (CD9: green), 0.5 μg ml^{-1} TH6-Alexa647 (JUNO: red), 1 μg ml^{-1} GoH3-Alexa546 (Integrin α6: purple) and 1 μg ml^{-1} Hoechst 33342 (nucleus: blue). Two different angles are shown of a latrunculin B-treated oocyte. Scale bars: 10 μm.

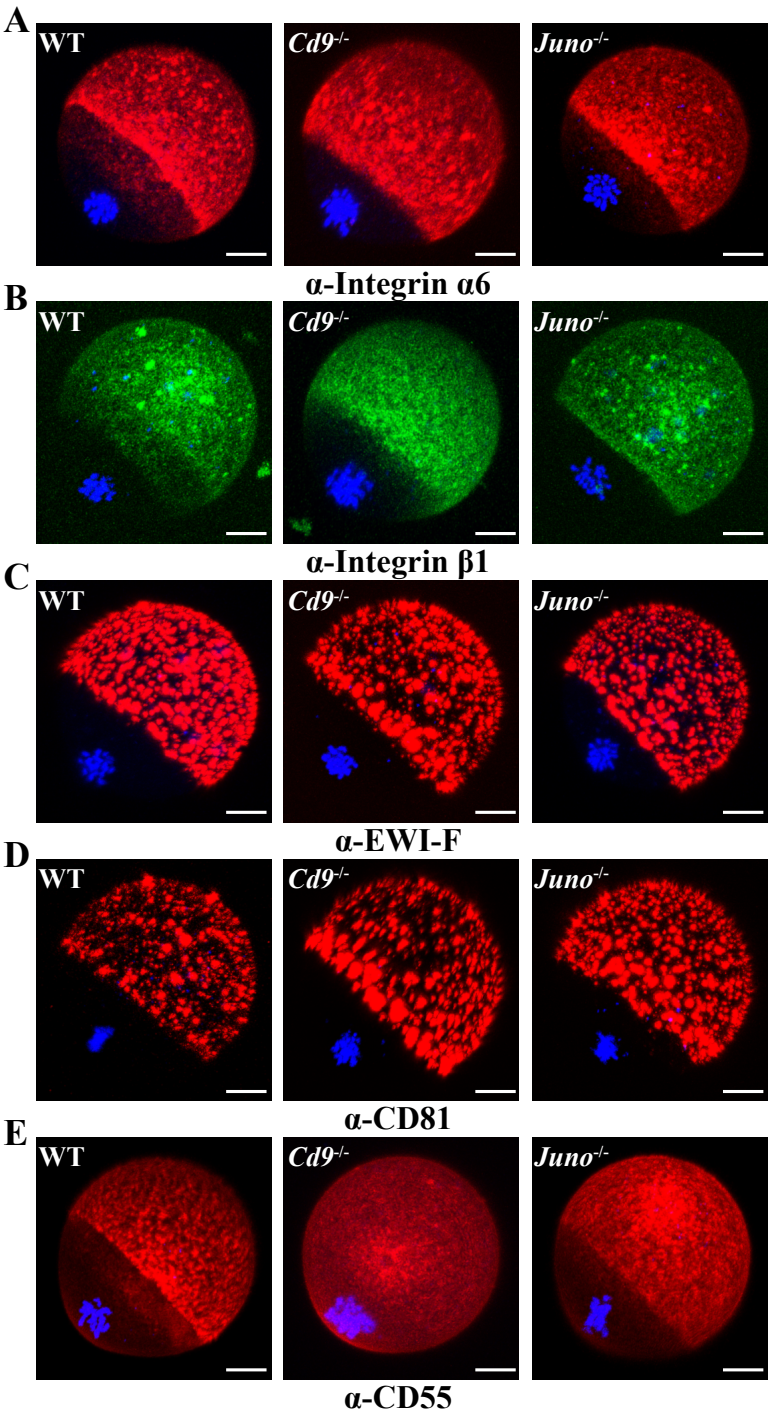

Fig. S2. Immunofluorescence of oocytes with antibodies against membrane-anchored proteins. WT, *Cd9*$^{-/-}$ and *Juno*$^{-/-}$ oocytes were incubated in TYH medium with 1 μg ml^{-1} GoH3-Alexa546 (Integrin α6: **A**), 5 μg ml^{-1} HMb1-1-FITC (Integrin β1: **B**), 2 μg ml^{-1} CD315 antibody (EWI-F: **C**, visualization: Alexa Fluor 647–labeled α-Sheep IgG), 5 μg ml^{-1} Eat2 (CD81: **D**, visualization: Alexa Fluor 647–labeled α-Armenian hamster IgG) and 1 μg ml^{-1} RIKO-3-Alexa647 (CD55: **E**). Scale bars: 10 μm.

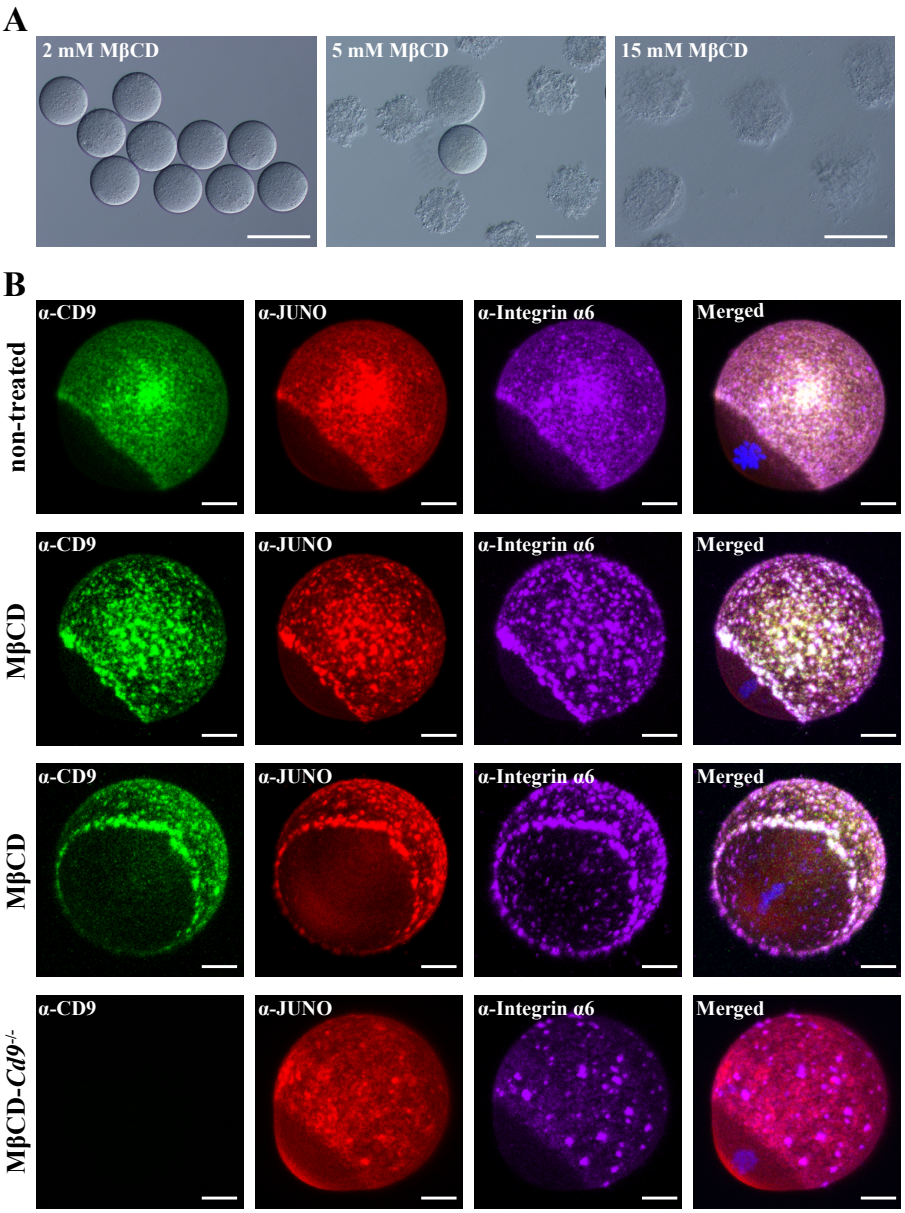

Fig. S3. Methyl-β-cyclodextrin (MβCD) treatment in oocytes.

(**A**) Cholesterol depletion of zona-free oocytes. The zona-free oocytes were incubated with different concentrations of MβCD for 30 min at 37°C. In this assay, all oocytes survived in the 2 mM MβCD treatment only. Scale bars, 100 µm. (**B**) Immunostaining analysis of oocytes after treatment with MβCD. The oocytes were incubated with 0.5 µg ml^{-1} MZ3-FITC (CD9: green), 0.5 µg ml^{-1} TH6-Alexa647 (JUNO: red), 1 µg ml^{-1} GoH3-Alexa546 (Integrin α6: purple) and 1 µg ml^{-1} Hoechst 33342 (nucleus: blue) in TYH medium for 90 min, then treated with 2 µM MβCD in FHM medium for 30 min. Two different angles are shown of a MβCD-treated WT and *Cd9*$^{-/-}$ oocytes. Scale bars: 10 µm.

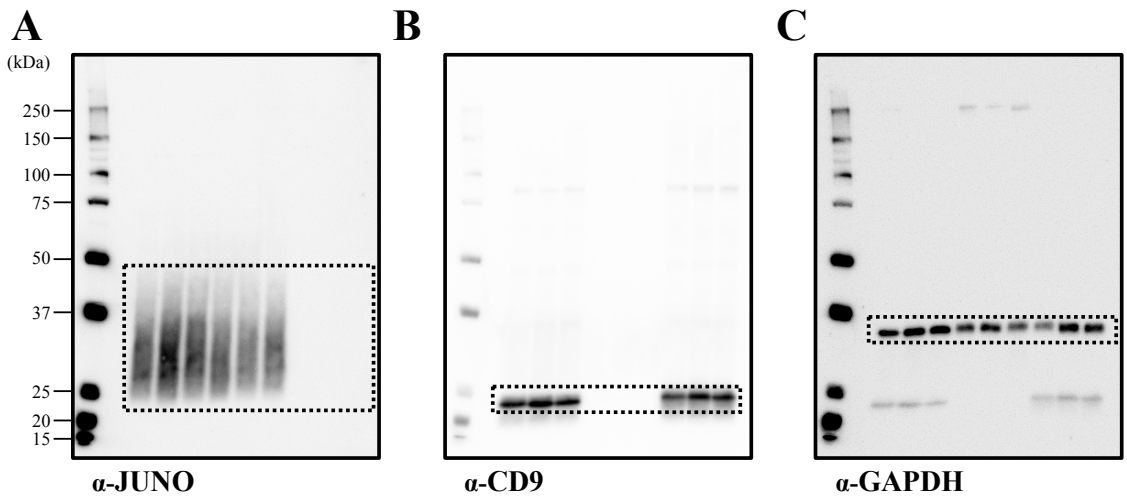

Fig. S4. Original western blot images.

Entire images of blots of Fig. 2B. Blots were incubated with 1 μg ml^{-1} 12A5 (JUNO: **A**), 1 μg ml^{-1} EM-04 (CD9: **B**) and 1 μg ml^{-1} 5A12 (GAPDH: **C**).

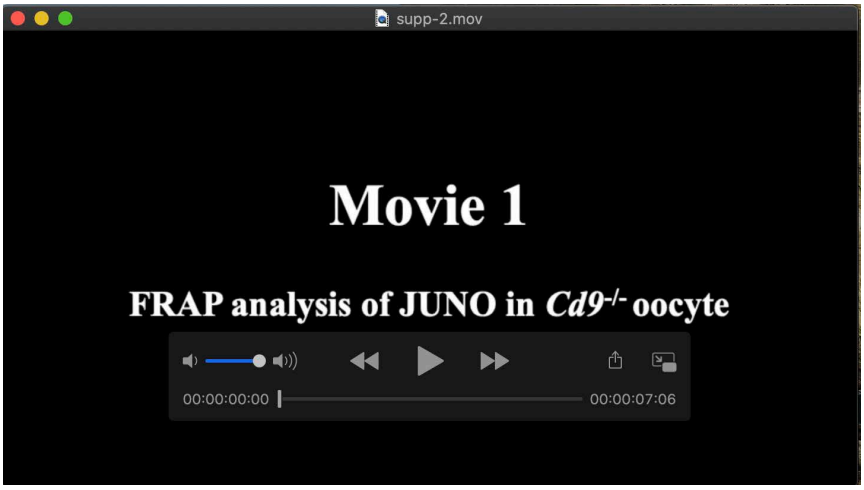

Movie 1. FRAP analysis of JUNO in *Cd9*$^{-/-}$ oocyte, related to Fig. 5B.

Oocytes are shown in Gray Scale (upper panels) and Fire LUT (bottom panels) of Fiji. The JUNO fluorescence images were taken at 2 min intervals over 58 min after photobleaching the cortical actin cap region.

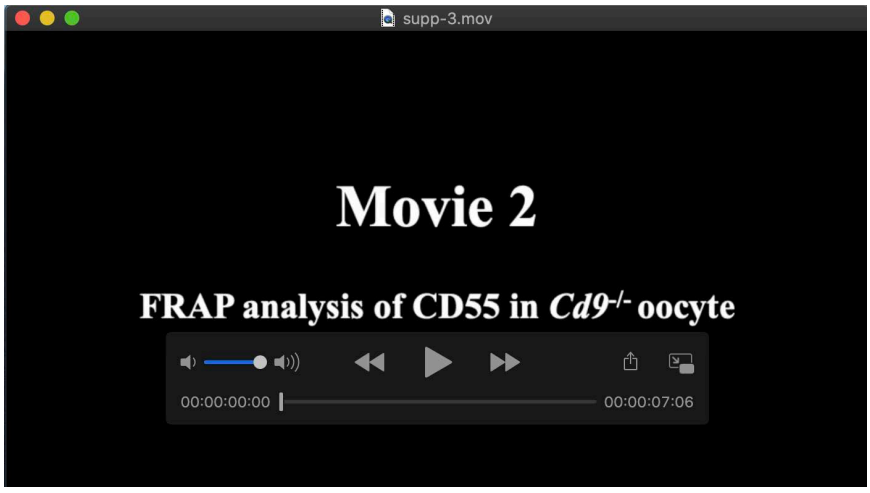

Movie 2. FRAP analysis of CD55 in *Cd9*$^{-/-}$ oocyte, related to Fig. 5B.

Oocytes are shown in Gray Scale (upper panels) and Fire LUT (bottom panels) of Fiji. The CD55 fluorescence images were taken at 2 min intervals over 58 min after photobleaching the cortical actin cap region.